HHS Public Access

Author manuscript

J Comp Neurol. Author manuscript; available in PMC 2019 August 02.

Published in final edited form as:

J Comp Neurol. 2017 April 01; 525(5): 1216–1233. doi:10.1002/cne.24131.

Nicotinic Acetylcholine Receptors Regulate Vestibular Afferent Gain and Activation Timing

Barbara J. Morley[1,*], **Anna Lysakowski**[2], **Sarath Vijayakumar**[3], **Deanna Menapace**[1], **Timothy A. Jones**[3]

[1]Boys Town National Research Hospital, Omaha, Nebraska 68131

[2]Department of Anatomy and Cell Biology, University of Illinois at Chicago, Chicago, Illinois 60612

[3]Department of Special Education and Communication Disorders, University of Nebraska, Lincoln, Nebraska 68583

Abstract

Little is known about the function of the cholinergic efferents innervating peripheral vestibular hair cells. We measured vestibular sensory evoked potentials (VsEPs) in α9 knockout (KO) mice, α10 KO mice, α7 KO mice, α9/10 and α7/9 double KO mice, and wild-type (WT) controls. We also studied the morphology and ultra-structure of efferent terminals on vestibular hair cells in α9, α10, and α9/10 KOs. Both type I and type II vestibular hair cells express the α9 and α10 subunits. The efferent boutons on vestibular cells in α9, α10, and α9/10 KOs appeared normal, but a quantitative analysis was not performed. Mean VsEP thresholds were significantly elevated in α9 and α9/10 KO animals. Some α9 and α9/10 KO animals, however, had normal or near-normal thresholds, whereas others were greatly affected. Despite individual variability in threshold responses, latencies were consistently shortened. The double α7/9 KO resulted in decreased variance by normalizing waveforms and latencies. The phenotypes of the α7 and α10 single KOs were identical. Both α7 and α10 KO mice evidenced normal thresholds, decreased activation latencies, and larger amplitudes compared with WT mice. The data suggest a complex interaction of nicotinic acetylcholine receptors (nAChRs) in regulating vestibular afferent gain and activation timing. Although the α9/10 heteromeric nAChR is an important component of vestibular efferent activity, other peripheral or central nAChRs involving the α7 subunit or α10 subunit and α9 homomeric receptors are also important.

[*]CORRESPONDENCE TO: Dr. Barbara Morley, Boys Town National Research Hospital, 555 North 30th St., Omaha, NE 68131. barbara.morley@boystown.org.

ROLE OF AUTHORS

All authors had full access to all the data in the study and take responsibility for the integrity of the data and accuracy of the data analysis. Study concept and design: all authors. Acquisition of physiology data: SV, TAJ. Acquisition of morphology images: AL. Drafting of the manuscript: BJM, TAJ, AL, DM. Critical revision of the manuscript for important intellectual content: BJM, TAJ, AL. Statistical analysis: TAJ. Obtained funding: BJM, AL, TAJ.

CONFLICT OF INTEREST STATEMENT

The authors have no competing financial interests.

Keywords

utricle; saccule; macula; latency; amplitude; evoked potential; efferent; RRID:AB_2079751; RRID:AB_90764; RRID:AB_2616561; RRID:SCK_002865; RRID:IMSR_JAX:000664; RRID:SCR_00207

The α9 and α10 nicotinic acetylcholine receptor (nAChR) subunits are members of the subfamily I, epithelial α9 and α10 ion-gated nicotinic receptor gene family. The α9 and α10 subunits are expressed in the epithelial cells of the vertebrate inner ear, including cochlear outer hair cells (OHCs) in the mature inner ear, cochlear inner hair cells (IHCs) in postnatal animals before the onset of hearing, and vestibular hair cells (Elgoyhen et al., 1994, 2001; Hiel et al., 1996; Vetter et al., 1999; Simmons and Morley, 2011). Alpha9 subunit expression has been reported in the lateral line of the trout (Drescher et al., 2004) as well as hair cells in the frog, fish, and turtle (Holt et al., 2006, 2015; Jordan et al., 2013); bird (Lustig et al., 1999); rodent (Elgoyhen et al., 1994; Luebke et al., 2005; Simmons and Morley, 2011); and human (Lustig and Peng, 2002).

The α9 and α10 subunits, in at least some species, can form homomeric receptors (Elgoyhen and Franchini, 2011). Functional mammalian α9 homomers have been demonstrated in Xenopus oocytes (Elgoyhen et al., 1994) and in the mouse cochlea (Vetter et al., 2007), but only the α9/10 heteromer is believed to transduce efferent signals in vivo in the cochlea (Elgoyhen et al., 2001; Vetter et al., 2007). The auditory and vestibular efferent neurons and boutons express presynaptic and postsynaptic cholinergic markers (Kong et al., 1994; Holt et al., 2011; Simmons and Morley, 2011), and the endogenous cholinergic receptor in the cochlea has a unique nicotinic pharmacology and physiology identical to that of the α9/10 receptor expressed in Xenopus oocytes (Elgoyhen et al., 1994, 2001; Holt et al., 2003).

Alpha9 and α10 nAChR subunit mRNA expression has been reported for both type I and type II vestibular hair cells (Hiel et al., 1996; Simmons and Morley, 2011). Cholinergic efferent axons terminate on type II hair cells as well as the innervating afferent boutons (Holt et al., 2011). Vestibular type I hair cells in the mature mammal, however, are innervated exclusively by a large afferent calyx (Wersäll, 1956; Lysakowski and Goldberg, 2004). These calyces are terminal endings on either calyx-only or dimorphic afferents. Calyx-only afferents are found in the central or striolar zone of vestibular sensory epithelia, whereas dimorphic afferents are found throughout the sensory epithelium where they contact both type I and type II hair cells. Finally, bouton-only afferents contact type II hair cells in the peripheral or extrastriolar zones (Fernandez et al., 1988, 1990). Cholinergic efferent axons terminate on the outer faces of the calyx, but not the type I hair cells directly (Holt et al., 2011). The expression of α9 and α10 in type I hair cells may be attributable to their early innervation by cholinergic efferent axons (Favre and Sans, 1979; Dechesne, 1992). It is not known whether the deletion of the α9 and/or α10 nAChR subunits affects the morphology or innervation pattern of vestibular boutons terminating on vestibular hair cells. It is also not known whether deletion of one or both subunits has a functional consequence. This study investigates the structure and ultrastructure of vestibular efferent boutons and the function of the vestibular afferents in mature wild-type (WT) C57Bl/6J and in mice with the deletion (knockout; KO) of the α9 nAChR subunit, the α10, or both the α9 and the α10

subunits (double KO). We investigated the possibility that residual 129/sv background genes might modify vestibular physiology in the knockouts. Finally, we investigated whether the deletion of the α7 nAChR subunit, which is heavily expressed in the vestibular brainstem (Happe and Morley, 1998), would modify vestibular physiology in the α9 KO.

MATERIALS AND METHODS

Animals

The α9 and α10 nAChR KO mouse models were generated by the deletion of exons 1 and 2 and their flanking intronic sequences (Genoway, Inc., Lyon, France). The embryonic stem cells used to make the transgenic mouse lines were from the 129/svPas (129S2; 129/sv) strain. The ATG translation initiation site and the stop codon are located in exons 1 and 5, respectively. There are no polymorphisms between the C57Bl/6J and the 129sv/Pas genetic backgrounds within the isolated nAChR α9 or α10 sequences. All aspects of the project were confirmed by PCR and Southern blot analysis. The F1 generation was genotyped by PCR and Southern blot.

The absence of gene transcript in the constitutive KOs was also verified by qPCR using Qiagen (Valencia, CA) PCR arrays (Fig. 1). Transcript was quantified in both WT and KO cochlear and vestibular tissues simultaneously using a customized Qiagen RT Profiler PCR array (SA Biosciences, Valencia, CA) and the Applied Biosystems (Foster City, CA) 700 Sequence Detection System. Cochlear and vestibular tissues, excluding the ganglia, from four WT, four α9 KO, and four α10 KO animals at P0 were dissected in RNALater (Life Technologies, Carlsbad, CA), and the tissue for each genotype was combined for processing. RNA was extracted and amplified using the recommended kits for the RT^2 Profiler PCR arrays (SA Biosciences), including RNeasy, the RT^2 First Strand kit, and RT^2 SYBR green, all according to the manufacturer's instructions. We sequenced the resulting products identified in WT tissue to confirm that the primers specifically recognized α9 and α10. With this technique, it is not uncommon for primers to recognize irrelevant transcripts in the absence of the intended transcript, e.g., gene deletion. When such PCR products were identified, they were sequenced and found to be transcripts that were recognized in the absence of the intended α9 or α10 transcript. The validity of the PCR arrays was confirmed by comparison with previous quantification of α9 and α10 transcripts using RT-PCR and in situ hybridization in the vestibule and cochlea at P0 (Simmons and Morley, 2011). The absence of α9 and α10 transcript and protein in cells dissected from the retina of the KOs used in this study was also recently reported (Smith et al., 2014).

The KO lines were back-crossed at the Boys Town National Research Hospital (BTNRH) to C57Bl/6J mice (Jackson Laboratory, Bar Harbor, ME) by using markerassisted accelerated backcrossing (MAX BAX; Charles River, Troy, NY) until congenicity (99%+) was achieved. For the studies reported here, mice were bred and housed at BTNRH until maturity, under presumed identical conditions. The α9 KO and WT mice were derived from heterozygote × heterozygote or heterozygote (female) × KO or WT (male) matings. Double KOs were derived from females and males heterozygous for either or both α9 and α10 and females heterozygous for α9 and KO for α10 and male double KOs. Neither the α9 nor α9/10 KOs has overt behavioral signs of a balance disorder.

The α7 nAChR strain was established from mice obtained from the Jackson Laboratories (JAX; https://www.jax.org, RRID:IMSR_JAX:000664) as heterozygote breeders after eight generations of back-crossing at JAX. The animals were then further back-crossed for four generations at BTNRH and have been periodically back-crossed with JAX WTs and KOs to prevent genetic drift. The α7 nAChR KO also has no observable gait or circling behaviors indicative of gross vestibular dysfunction.

The litter sizes for all strains varied from six to nine (litters larger than nine were culled to nine at birth). Dams and males in our colony are typically first bred at 6-8 weeks of age, not used for more than two litters, and not bred past the age of 12-14 weeks. Young dams and males are used for breeding to reduce the incidence of epigenetic factors that might affect the phenotype.

Twelve WT, α9 KO, and double α9/10 KO male or female animals, aged 7-9 weeks, were prepared for structural analysis of the vestibular organs. The tissue was fixed by transcardiac perfusion, as described below, at BTNRH and shipped to the University of Illinois at Chicago (UIC) for processing and analysis.

Forty-four wild type, 28 α9 KO, 15 α9/10 double KO, 20 α7/9 double KO, 14 α7 KO, and 18 α10 KO male or female mice were tested for vestibular function. Eighty-two female and fifty-seven male mice were used in these studies. The animals used for physiology studies were transferred from BTNRH to the University of Nebraska at Lincoln (UNL) by common courier in a temperature-controlled van and were in transit for approximately 1.5 hours. The animals were acclimated at the UNL laboratory for approximately 1 week before testing. Not all of the animals were tested at the same time. For the α9 and double α9/10 experiments, there were three shipments over a period of 9 months. Animals with α7 and α10 single deletions and WT controls were assessed in a single separate experiment. There were no significant differences between animals of the same genotype, including WT controls, tested on differ-ent dates. The mean age of animals in the physiology experiments, when tested, was 1.9 ± 0.4 months (n = 149). All procedures used for this study followed NIH guidelines and were approved by the institutional animal care committees at BTNRH, UIC, and UNL

Morphology

WT and α9, α10, and α9/10 KO mice were fixed by transcardiac perfusion with a solution of phosphate buffer (PB; pH 7.4) and 1% sodium nitrite, followed by 4% paraformaldehyde/5% sucrose in 0.1M PB (pH 7.4) for light microscopy or 3% paraformaldehyde/2% glutaraldehyde/5% sucrose for transmission electron microscopy (TEM). Tissue for light microscopy was postfixed for 2 hours, stored in buffer overnight, and processed on the next day. Tissue for TEM was stored in fixative until processing. Details on EM preparation have been given by Lysakowski and Goldberg (2008).

Efferent terminals were identified with a 1:200 dilution of a polyclonal goat anti-ChAT (EMD-Millipore, Chemicon, Temecula, CA; AB144P, lot No. NG1915294, RRID:AB_2079751). The antibody was generated in goat against the enzyme isolated from human placenta and has been confirmed specifically to label choline acetyltransferase by

Western blot. The antibody labels a 70/74-kDa band consistent with the molecular weight of choline acetyltransferase in mouse brain (Jordan et al., 2015). Calyx afferents were labeled with a 1:200 dilution of a polyclonal goat anti-calretinin (EMD-Millipore, Chemicon; AB1550, lot No. 060302, RRID:AB_90764). This antibody has been confirmed specifically to label calretinin by Western blot. The antibody labels a 31.4-kDa band consistent with the molecular weight of calretinin in mouse brain (Liu and Davis, 2014). The antibody labels the calyx-only afferents in the mouse vestibular end organs (Desai et al., 2005) A 1:800 dilution of a custom polyclonal anti-rabbit otoferlin antibody was used to mark vestibular hair cells (Thermo Fisher Scientific, Fair Lawn, NJ; catalog No. Custom_MorBar_001, RRID:AB_2616561). This antibody was confirmed specifically to label otoferlin by Western blot. The antibody labels a single band consistent with the predicted molecular mass of 227 kDa of otoferlin, specifically labels vestibular hair cells using immunfluorescence (Ramakrishnan et al., 2014), and labels hair cells identically to labeling in previous in situ hybridization studies (Schug et al., 2006). The controls for all antibody labeling were normal goat serum (ChAT, calretinin), absorption control (ChAT), or normal or preimmune rabbit serum (otoferlin; see Table 1).

Immunoreacted 35-μm frozen sections for confocal microscopy were examined at an optical section thickness of 0.5 μm on a laser scanning confocal microscope (LSM 510 Meta or LSM 710; Zeiss, Oberköchen, Germany). Transmission electron micrographs were taken on a JEOL 1220 electron microscope (JEOL, Peabody, MA). Figures were prepared in Adobe Photoshop CS4 Extended, v.11.0.2 (Adobe Systems Inc., San Jose, CA; RRID:SCR_00207). The images were not altered.

Vestibular sensory evoked potentials

Immediately prior to vestibular sensory evoked potential (VsEP) testing, mice were deeply anesthetized by intraperitoneal injection of ketamine/xylazine (18:2 mg/ml; 5-7 μl/g body weight), followed by maintenance doses of 0.05 ml; every 60 minutes as needed to maintain adequate anesthesia throughout testing. Core body temperature was maintained at 37.0 °C 6 0.2 °C with a homeothermic heating blanket. VsEP recordings were based on methods published previously (Jones et al., 1999, 2004, 2015; Mock et al., 2011). Briefly, vestibular stimuli (linear head translations) were delivered by securing the mouse head to a mechanical shaker (model ET-132203; Labworks Inc., Costa Mesa, CA) using a noninvasive head clip (Fig. 2). Linear acceleration ramps (17 pulses/second, 2 msec duration) were used to generate rectangular (step) jerk stimuli specified in units of g/msec, where 1 g = 9.8 m/sec^2, that were in turn applied to the head. Jerk stimuli ranged in amplitude from +6 to −18 dB re: 1 g/msec and were adjusted in levels of 3 dB. Stimuli were presented to the head in the naso-occipital axis, thus stimulating both saccular and utricular receptors. Stimulus levels were also expressed relative to each animal's threshold in decibel sensation level (SL). This represents the number of decibels above each animal's threshold.

Subcutaneous needle electrodes were placed posterior to the right pinna and at the right hip for inverting and ground electrodes, respectively. Stainless-steel wire placed subcutaneously at the nuchal crest served as the noninverting electrode. Electroencephalographic activity was amplified (×200,000), filtered (300-3,000 Hz), and digitized (1,024 points at 10 μsec/

point). Two hundred fifty-six primary responses were averaged and replicated for each VsEP waveform. A VsEP intensity series was collected beginning at the maximum stimulus level (i.e., +6 dB re:1 g/msec) with and without acoustic masking (50-50,000 Hz forward masker at 90 dB SPL), and then stimulus levels were increased from −18 dB to + 6 dB re:1 g/msec in 3-dB steps to determine vestibular response thresholds. Threshold was defined as the stimulus level halfway between the highest level failing to produce a response and the lowest level producing a response.

The first three VsEP positive (p) and negative (n) response peaks were scored and labeled sequentially from the earliest to latest, p1, n1, and p2, respectively. Latency was defined as the elapsed time from the stimulus onset to the scored response peak (msec). Response amplitudes were defined as the amplitude of the positive peak (in μV) minus the amplitude of the negative peak. These provided response measures for peripheral (p1, n1) and central (p2) response latencies as well as peripheral (p1n1) and central (p2n1) response amplitudes (Nazareth and Jones, 1998). These response metrics and threshold were used to evaluate the effects of genotype.

Genome scan

The genome scan was conducted on DNA from eight animals. The genetic background strain genes flanking the transgene insertion sites in α9 and α10 genes were determined in KO animals that had either normal or near-normal (“best”) or most abnormal (“worst”) thresholds. Strain background characterization was achieved by microsatellite analysis (Charles River, Troy, NY). The PCR-based method was used to scan the X chromosome and all 19 autosomes of the mouse genome at approximately 15-cM intervals (resulting in 384 SNP markers) to identify regions of 129sv background flanking the transgene insertion site α9 gene in the KOs and both the α9 and the α10 insertion sites in the double KO.

Statistical analysis

Univariate and multivariate analyses of variance (ANOVA and MANOVA, respectively) were used to evaluate the effects of genotype on response parameters (SPSS for Windows, v. 22; SPSS, Chicago, IL; RRID:SCK_002865). The response parameters between male and female animals were not significantly different, and the data were combined for analysis. Least significant difference (LSD), Bonferroni, and Tukey tests were used for post hoc evaluation. Repeated measures MANOVA (rmMANOVA) was employed to evaluate the influence of genotype on responses to multiple stimulus levels. To preserve sample sizes during repeated-measures analysis, we evaluated the three stimulus levels giving the largest sample sizes across all genotypes. These were 0, +3, and +6 dB re:1 g/msec for absolute levels and +7.5, +10.5, and +13.5 dB SL for sensation level. Mean and standard deviation (SD) or standard error (SE) and sample size (n) were used to report descriptive statistics in the form of mean ± SD (n), unless otherwise stated.

RESULTS

Confocal microscopy

Otoferlin, a transmembrane-anchored fusion protein expressed by vestibular hair cells, was used as an antibody marker to identify vestibular hair cells. Otoferlin immunostaining appeared more intense in type II hair cells than in most type I hair cells (Fig. 3) in the WT and α9 and α10 KO mice. The significance of the apparent difference between type I and type II hair cells in immunolabeling is not known. Several of the type II hair cells had extensive foot processes, as has been previously described (Pujol et al., 2014). Thus, there were no apparent structural differences in the hair cells between WT and the KO mice at the confocal level.

ChAT was used as an antibody marker for efferent boutons, in combination with calretinin, which labeled *extrastriolar* type II hair cells and *striolar* calyces, providing a marker for the striolar region as described previously (Desai et al., 2005). Efferent boutons were similar in size and appearance in both the WT and the α9 KO mice at the confocal level (Fig. 4). They were not displaced above their normal location at the basal end of the hair cell, in contrast to what has previously been described for the cochlea (Vetter et al., 2007; Morley and Simmons, 2012; Morley et al., 2012).

Electron microscopy

Our ultrastructural results showed no obvious differences between the WT controls and the various KOs (Fig. 5). Hair cells, supporting cells, calyces, and afferent and efferent boutons in all samples appeared normal, based on comparison with EM data from WT mice and other species (Lysakowski, 1996; Lysakowski and Goldberg, 1997, 2008; Holt et al., 2006, 2011). Typical features of vestibular sensory epithelium cytoarchitecture, such as the placement of type II hair cell nuclei above those of type I nuclei, the location of efferent and afferent boutons at the base of hair cells and calyceal endings, the normal extent of myelin below the sensory epithelium, normal hair bundles, normal arrays of stereocilia, etc. (Lysakowski, 1996; Lysakowski and Goldberg, 1997, 2008; Holt et al., 2006, 2011), were all observed. In WT control mice (Fig. 5A), examination of sectioned material revealed efferent synapses with normal synaptic vesicles, normal synaptic specializations such as postsynaptic densities in afferent endings and subsurface cisterns in type II hair cells, as well as normal synaptic ribbons in hair cells. For the α9 KO (Fig. 5B) and α10 (Fig. 5C) mice, results were similar. The double α9/α10 KO mouse (not shown) was similarly unremarkable in terms of ultrastructure.

Physiology

The linear VsEP is a compound action potential produced by eighth nerve neurons innervating gravity receptors (otoconial organs) and their central relays in the brainstem (Nazareth and Jones, 1998; Jones et al., 1999, 2004; Jones and Jones, 2014). Figure 6 illustrates representative VsEP responses to stimulus levels of +6 dB re:1 g/msec (maximum level) for sibling WT, α9 KO, α9/10 KO, and α7/9 KO animals. WT animals (top five response trace pairs) demonstrated typical VsEP responses comparable to those of standard control C57Bl/6J mice obtained directly from the Jackson Laboratory (Bar Harbor, ME).

Similarly, α7/9 KO animals (bottom five response trace pairs) had VsEP response waveforms like those of WT animals with well-defined consistent peaks and relatively low variability. Although not shown, VsEP responses in α7 KO and α10 KO animals were similar in morphology and variance to those of WT controls and α7/9 KO animals shown. In contrast, VsEPs for other KO groups (α9 and α9/10 KOs) were often poorly formed and highly variable, having reduced amplitudes and altered latencies. In two cases (Fig. 6, α9 KO group, trace pairs 2 and 5), responses were absent (α9 KO, 2048) or virtually absent (α9 KO, tm07). Both the α9 KO and the α9/10 double KO groups had significantly elevated thresholds on average compared with WT mice (Fig. 7, Table 2), suggesting significantly reduced sensitivity of the macular epithelium in α9 KO and α9/10 KO animals. Consistent with this was the finding that response amplitudes at the highest stimulus level (Fig. 8A, Table 2) as well as across the highest three levels (levels 0, +3, and +6 dB re:1 g/msec; Fig. 8C,D) were reduced for both peripheral and central peaks in α9 KO and α9/10 KO groups only. Response thresholds and peripheral amplitudes at the highest levels (0, +3, and +6 dB re:1g/msec) for the α7 KO, α10 KO, and α7/9 KO groups were not significantly different from WT (Figs. 7 and 8A; +6 dB re:1 g/msec only). Neural activation latencies (p1, n1) for knockout groups were either the same as, or significantly shorter than, WT at the highest stimulus level (see Fig. 8B, Table 3) as well as across the three highest stimulus levels (0, +3, and +6 dB re:1 g/msec). This was an unexpected finding given the elevated thresholds for α9 KO and α9/10 KO animals and represented a response feature suggesting altered timing of neural activation. Elevated thresholds and reduced amplitudes are normally associated with prolonged latencies. Amplitudes for the α9/10 KO animals tended to be less than those for α9 KOs (Fig. 8A), whereas there were no differences between the α9 KO and the α9/10 KO groups in response thresholds or latencies (Figs. 7 and 8B, Tables 2 and 3).

The relationship between stimulus input and response output was evaluated for response amplitudes and latencies. As in all normal strains, response latencies decreased and amplitudes increased with increasing stimulus level for all genotypes studied here. These relationships were highly significant and can be appreciated from Figures 8C,D, 9, 10 and 12. Response values were normalized for threshold differences across animals by plotting values as a function of stimulus sensation level in dB SL Figs. 9, 10 and 12. This representation underscores effects that are not associated with the threshold changes reported above. Although substantially lower amplitudes were present in both α9 KO and α9/10 KO groups at the highest stimulus levels (as noted above; see Figs. 8A,C,D), the effects of genotype on response amplitudes remained highly significant only for the α9/10 KO group when threshold was taken into consideration (Fig. 9A,B; rmMANOVA, $F_{10,222}$ = 4.00, P = 4.7×10^{-5}; LSD: α9/10 KO p1n1: P = 0.00027, p2n1: P = 0.0022). This is also apparent in Figure 11A, representing amplitudes for all genotypes at the single stimulus level of +10.5 dB SL (α9/10 KO, p1n1: MANOVA, $F_{10,238}$ = 3.551, P = 2.12×10^{-4}; LSD: P = 0.0012). These results suggest that amplitude effects were largely, but not entirely, associated with threshold elevation. Remarkably, latency effects found at the highest stimulus level (Fig. 8B), and across several absolute stimulus levels for some KO groups noted above, were actually more clearly resolved and evident in most KOs when threshold was taken into consideration (Fig. 10A,B; rmMANOVA, $F_{15,333}$ = 5.04, P = 5.48×10^{-9}; LSD: n1: α9 KO, P = 1.8×10^{-3}, α9/10 KO, P = 6.5×10^{-3}), indicating that the

significantly shorter latencies were not related to threshold changes. This can also be seen in Figure 11B showing normal, or significantly shorter, n1 latencies for all KO animals at a stimulus level of +10.5 dB SL (MANOVA, $F_{15,357} = 4.50\ 5$, $P = 7.65 \times 10^{-8}$). One additional feature of the latency profiles is that the mean interpeak latency between p1 and n1 (latency of n1 minus p1) was shorter than that of WT, but only in α9 KO and α9/10 KO mice (Fig. 10A,B; MANOVA, $F_{10,238} = 3.71$, $P = 1.20 \times 10^{-4}$; LSD: α9 KO, P = 0.004, α9/10 KO, P = 0.0029), whereas the interpeak latency between p2 and n1 was not different from WT for any genotype. This suggests that latency effects were restricted primarily to the periphery and, for α9 KO and α9/10 KO mice, may include effects within primary afferent neurons themselves, such as altered channel kinetics associated with the action potential itself (e.g., Na^+, K^+).

There were no differences in thresholds (Fig. 7), amplitudes (Figs. 8A,B, 9C, 11A), or latencies (Figs. 10C, 11B) between WT and α7/9 KO animals for any stimulus condition. Indeed, responses in α7/9 KO animals were indistinguishable from those of normal WT animals.

The α7 KO and α10 KO animals had robust VsEP responses. Although thresholds were normal in α7 KO and α10 KO animals, their mean latencies were shorter than in WT animals (Figs. 8B, 11B, 12A,B, Table 3). Unlike α9 KO and α9/10 KO mice, the shorter latencies were not accompanied by shorter interpeak latencies in α7 KO and α10 KO animals. Response amplitudes for α7 KO and α10 KO groups, although quite robust, were not significantly different from WT.

Genome scan

The results of the strain characterization are shown in Figure 13. The residual 129/sv genes flanking the α9 and α10 genes for the animals with the “best” and “worst” VeSPs did not differ. The results for the animals with the best threshold (animal 2038) and worst threshold (animal 2012) were identical (Fig. 13).

DISCUSSION

The data reported here suggest that multiple nAChRs are involved in the regulation of vestibular efferent activity. Of particular interest are the different phenotypes found for the α7, α9, α10, and α9/10 KO mice. It is widely assumed that α9 assembles with α10 wherever α9 expression is found. As a result, the nomenclature α9/10 or α9* is often used even when α10 expression is not measured. As a result, few studies have focused on the α10 subunit, and it has been referred to as a “structural” subunit, analogous to the nAChRb subunits (Plazas et al., 2005). Our data suggest that this might not always be the case.

Alpha9 and α10 pentameric homomeric receptors with similar properties resulted from a primordial gene by duplication and an early split (Le Novere and Changeux, 1995). The α9 and α10 subunits both possess adjacent cysteines, which are a hallmark requirement for agonist binding in members of the Cys-loop ligand-gated ion channel superfamily (Karlin, 2002). Although the sequence of the α9 subunit is generally conserved, three amino acid nonsynonomous substitutions in the mammalian gene have rendered the mammalian α9

homomer and the α9/10 heteromeric receptor highly permeable to calcium. These nonsynonomous substitutions do not result in high calcium permeability in the homologous avian receptors (Lipovsek et al., 2014).

The α10 subunit has undergone positive Darwinian selection in mammals, paralleling the evolution of the anion chloride transporter SLC26A5 (prestin) and somatic electromotility in cochlear OHCs (Franchini and Elgoyhen, 2006; Elgoyhen and Franchini, 2011). Although the avian α10 formed a functional homomer when cRNA was injected into oocytes (Lipovsek et al., 2014), the mammalian α10 did not (Elgoyhen et al., 2001; Lipovsek et al., 2014). The consequences of the positive selection of α10 are, therefore, not completely understood (Lipovsek et al., 2014). One possible function may involve calcium permeability, either as an α10 homomer or assembled with another nAChR subunit.

In the cochlea, α9 expression has longitudinal and radial gradients, with greatest expression over OHCs in the basal region (Simmons and Morley, 1998), suggesting a higher density of nAChRs in the high-frequency region of cochlea where low-calcium affinity, large-conductance BK channels (in addition to the small-conductance SK channels in apical OHCs) are required for activation (Lipovsek et al., 2012). Thus, the mammalian α9/10 nAChR in the cochlea is uniquely adapted to modulating OHC somatic electromotility.

Because somatic electromotility is not observed in vestibular hair cells and prestin expression has a more diffuse localization than in cochlear OHCs (Adler et al., 2003), specific functions of the α9* or α10* nAChRs likely differ between vestibular and cochlear hair cells. In addition to the importance of studying the cholinergic efferent innervation of vestibular hair cells, understanding how the α9 nAChR functions in these cells may also have relevance to the low-frequency apical region of the mammalian cochlea (Rabbitt and Brownell, 2011).

For the cochlea, the existence of α9 homomeric receptors has been reported but subsequently has been given little attention (Vetter et al., 2007). The small ACh-evoked currents in the cochlea of α10 KOs may be insufficient to drive normal olivocochlear efferent function (Vetter et al., 2007).

An important observation in the current study is that the efferent boutons in α9, α10, and α9/10 mice terminating on vestibular type II hair cells and the calyx innervating type I hair cells were not displaced, as has been reported for the cochlea of mice with both B6.CAST-ahl^{+} and C57Bl/6J backgrounds (Vetter et al., 2007; Morley and Simmons, 2012; Morley et al., 2012). At the light microscopic level, using immunohistochemistry, and at the ultrastructural level, there were no observable differences in the location of efferent boutons terminating on type II vestibular hair cells. Dimorphic afferent boutons contacting type II vestibular hair cells also appeared normal.

Despite the apparent normal overall structure of efferent innervation, we nonetheless found that the deletion of the nAChR subunits resulted in similar, but not identical, physiological consequences. The most parsimonious interpretation of the physiological measurements in α9* KOs is that the nicotinic cholinergic component of the vestibular efferent system has a role in modulating afferent activity. Activation of efferent projections to vestibular sensors is

known to alter both spontaneous discharge activity and the gain exhibited by primary vestibular afferents in response to head motion (see, e.g., Holt et al., 2011; discussed below).

The decreased vestibular sensitivity shown here for α9 KO and α9/10 KO mice is consistent with a loss of function in the form of a reduced sensitivity of the macular neuroepithelium to transient head motion. The finding of normal or shorter VsEP latencies is interesting in that it implies further that deleting the α9 or α9/10 nAChR alters the timing of neural activation beyond what a threshold change alone would produce. A threshold elevation normally produces prolonged latencies, yet here latencies for α9 KO and α9/10 KO mice were not prolonged (e.g., Fig. 8B). Presumably, this requires an enhancement of stimulus-triggered neural spike onset timing. Such an effect is independent of threshold inasmuch as it was also present when latencies were expressed in terms of dB SL (Figs. 10A,B, 11B). A similar decrease in onset latencies also occurred in the α7 KO and α10 KO mice, which notably had normal thresholds (Figs. 7B, 11B, 12A,B).

The unusual occurrence of shortened p1n1 interpeak latencies is of interest because it suggests altered processes within the vestibular primary afferent itself. The response peaks p1 and n1 are both generated by the synchronous activation of gravity receptor primary afferents (Nazareth and Jones, 1998), which produces the resulting compound action potential (CAP) recorded in the far-field at the surface of the skull. Whether the two electrical reversal points (peaks p1 and n1) reflect two different regions of the nerve or two different temporal aspects of the CAP is not clear. In either case, the changes reflect an altered time course of the CAP, whether from changes in conduction velocity or duration of the action potential discharge. Thus, the shorter interpeak latencies found only in α9 KO and α9/10 KO mice may reflect altered primary afferent membrane channel kinetics (e.g., Na^+ and/or K^+), which could explain either of these cases.

The phenotypes of the α9 KOs and double α9/10 KOs were in the same direction, but the effects in the double KO were generally of greater magnitude. Both the α9 KOs and the α9/10 KOs had reduced p1n1 and p2n1 amplitudes (Fig. 8A,C,D); however, amplitudes for α9 KOs were significantly larger than α9/10 KOs (Fig. 8A,C,D).

An interesting aspect of the VsEP phenotype was the high variability in thresholds found only in α9 and α9/10 KOs. Although some of the α9 and α9/10 KO animals had normal or near-normal thresholds, others had “flat” waveforms. Variance observed in inbred mice may be attributable to residual genes from the original background strain. Using a genome scan with 384 SNPs, we found that the best and worst of the α9 KO and α9/10 double KO animals tested could not be distinguished from each other by the residual 129/sv background. Variance in inbred strains can also be of environmental or epigenetic origin (Lathe, 2004). The source of an environmental or epigenetic factor affecting vestibular function is not intuitively obvious. In our study, the animals were bred and housed in a defined environment to decrease variability, i.e., young dams, similar litter size and age, animals/cage, and diet. Additionally, in one case, animals in the best and worst threshold groups were from the same litter (animals 2012 and 2013).

The observed variation in thresholds may have an origin in efferent disinhibition and dysregulated efferent cholinergic excitatory processes. Recent evidence indicates that the α9* nAChR mediates efferent-induced inhibition of the type II vestibular hair cell (Holt et al., 2011, 2006, 2015; Kong et al., 2007; Jordan et al., 2013) and likely plays essentially no direct role in mediating efferent cholinergic excitation of vestibular primary afferents (Holt et al., 2015). Instead, stimulation of vestibular efferent projections to the vestibular neuroepithelium is thought to initiate distinct simultaneous inhibitory and excitatory actions on the vestibular apparatus normally; although in mammals this dual action consistently results in a net excitation of vestibular primary afferents (see, e.g., Goldberg and Fernandez, 1980; Holt et al., 2011; McCue and Guinan, 1994; Marlinski et al., 2004). If the absence of the α9*nAChRs is viewed as a disinhibition in vestibular efferent action, one would predict a resulting marked excitation of vestibular sensors (most notably dimorph afferents via disinhibited type II hair cells), and such an outcome could in some way contribute to the shortened VsEP onset latencies (enhanced activation timing) found for α9 and α9/10 KOs.

Conceivably, in the absence of α9 and α9/a10 inhibitory action, the more prominent efferent excitatory processes might also provide an explanation for the varying thresholds found in the present study. Fast (mediated by α4/β2* or α6/β2* nAChRs) and slow (mediated by mAChRs 1, 3, and 5) excitatory vestibular efferent processes have been described and are thought to mediate, respectively, decreases and increases in primary afferent gain following efferent activation (Holt et al., 2011, 2015; Jordan et al., 2013). It is possible that under normal circumstances the balance between fast and slow efferent cholinergic excitation is adjusted and sets the sensitivity of vestibular epithelia to natural stimulation.

VsEP threshold reflects the overall sensitivity of the macular epithelium to transient stimulation. Vestibular afferents thought to respond to such transients are irregular fibers including both dimorph and calyx afferent types. The elevated VsEP thresholds reported here for α9/α10 KOs could be explained by a reduced responsiveness to high-frequency events and/or a shift to less dynamic response characteristics in the afferents normally generating the VsEP. A shift to more regular discharge characteristics for the population would accomplish the latter outcome. Consistent with this hypothesis is the finding of a reduced proportion of irregular fibers in α9 KO mice reported by Han et al. (2007).

The idea of a change in discharge regularity for a large number of cells in a population of vestibular afferents has been entertained previously by others. An apparent population shift in the proportion of irregular and regular vestibular afferent fibers following unilateral labyrinthectomy was reported by Sadeghi et al. (2007), and these investigators argued that efferent activity might have mediated such changes during compensation to the injury. Hübner et al. (2015) also suggested that the excessive activity of disinhibited type II hair cells in an α9 KO could mediate a shift to more regular discharge activity in dimorph afferents. An additional efferent mechanism may also contribute to a change in discharge regularity. The action of slow efferent excitation is mediated by mAChRs (Jordan et al., 2013), which when activated inhibit low-voltage-activated K^+ currents (I_{LV}) in calyx and dimorph afferents (Selyanko et al., 2000; Kalluri et al., 2010). Reduction of I_{LV} in turn leads directly to a shift to more regular, sustained firing patterns in calyx and dimorph afferents in

vitro (Iwasaki et al., 2008; Kalluri et al., 2010) and would hypothetically reduce responses to transient stimuli and increase VsEP thresholds in intact animals.

Opposing actions of fast and slow efferent activity on afferent dendrite membrane time constants could either enhance the transfer of high frequencies (reduce membrane time constant, fast α4/α6/β2) or reduce high frequency transfer (increased membrane time constant, mAChR) to postsynaptic membranes depending on the balance of fast and slow efferent action. Reduced high-frequency transfer from hair cell to postsynaptic afferent would also serve to reduce VsEP responses.

Thus the reduced sensitivity to transient stimuli and accompanying elevated VsEP thresholds observed here in α9 and α9/10 KOs could at least in part result from an abnormal balance in fast and slow efferent activity. Indeed, the wide variation in thresholds could reflect varying dominance of the fast and slow efferent processes across animals, suggesting that the inhibition mediated by α9* nAChR might normally have a stabilizing influence on the balance of fast and slow excitatory efferent mechanisms. Some of these notions, although plausible, are based on studies in nonmammalian species, and all hypotheses remain to be critically evaluated in the mammal.

With regard to α9/α10 mechanisms of inhibition, the published work on turtle and frog extrapolated receptor subunit composition assumed the receptor was α9/10 primarily on the basis of pharmacology. Calcium permeability of the α9* receptor in nonmammals is low and is similar to that of the α4β2 receptor (Lipovsek et al.,2014, although the pharmacology of the α9/10 in both species is similar (see, e.g., Holt et al., 2011, 2015). The pharmacological profiles of the mammalian α9 homomer and the α9/10 heteromer are also similar even though the biophysical properties are different (Elgoyhen et al., 1994, 2001). Thus, nAChR mediating minimal Ca^{2+} current may contribute to the activation of potassium channels by acting through, or in synergy with, voltage-sensitive L-type calcium channels (Kong et al., 2007; Schweizer et al., 2009). BK and SK potassium channels and calcium channels have been identified in type II vestibular hair cells (see, e.g., Kong et al., 2007).

Our data suggest that nicotinic cholinergic responses in the vestibular system are mediated by a complex interaction of several subunits. The deletion of the α9 and α10 subunits eliminates both α9 homomers and α9/10 heteromers and should therefore have the most pronounced effect on the phenotype, and it does. The deletion of the α9 subunit should, theoretically, produce the same phenotype as the double α9/10 KO, but it does not, suggesting that the α10 subunit functions as a homomer or as a heteromer assembled with a different subunit. The deletion of the α10 should have the same effect as α9 deletion, but it does not, presumably because it leaves α9 homomeric receptors intact. Oocytes injected with rat α10 in combination with α1-6 or β1-4 DNA fail to form a functional receptor (Elgoyhen et al., 2001). The coinjection of α7 and α10 has not been reported. Alpha7* receptors are not known to be expressed in either cochlear or vestibular hair cells, at least at an age when they might function at synapses (Hiel et al., 1996; Morley et al., 1998). Although surprising, our data support the hypothesis that the α10 subunit has a physiologically relevant function in the absence of the α9 subunit, at least in the vestibular system.

Because the α7 nAChR is heavily expressed in Scarpa's ganglion and central vestibular nuclei (Hiel et al., 1996; Happe and Morley, 1998), we tested animals deleted for α7 (α7 KO) and both α7 and α9 (double α7/9 KO). The deletion of α7 alone produced decreased latencies, like the α9* deletions. Unexpectedly, the deletion of the α7 subunit normalized the α9 KO phenotype (Figs. 6-11; α7/9 KO). One interpretation of these data is that the α7* receptors and α9* receptors balance vestibular activity, possibly through central mechanisms.

In summary, the data suggest a complex interaction of nAChRs in regulating vestibular afferent gain and activation timing. Although the α9/10 heteromeric nAChR is an important component of vestibular efferent activity, as it is in the cochlea, other peripheral or central nAChRs involving the α7 subunit or α10 subunit and α9 homomeric receptors are also important. The alteration of the physiological responses does not correlate with structural aberration of the efferent innervation, but further studies may reveal subtle changes in morphology or changes in molecular synaptic mechanisms not evident in morphology.

ACKNOWLEDGMENTS

We thank Mr. Steven D. Price for excellent technical support. We thank Dr. Yunxia Wang Lundberg at the Boys Town National Research Hospital for her assistance in dissecting some of the vestibular samples.

Grant sponsor: Nebraska Tobacco Settlement Biomedical Research Foundation (to B.J.M., T.A.J.); Grant sponsor: Deafness Research Foundation, American Hearing Research Foundation (to B.J.M.); Grant sponsor: National Organization for Hearing Research (to B.J.M.); Grant sponsor: National Institutes of Health; Grant numbers: R01 DC006907 (to B.J.M.); R01 DC002058 (to A.L.).

LITERATURE CITED

Adler HJ, Belyantseva IA, Merritt RC Jr, Frolenkov GI, Dougherty GW, Kachar B. 2003 Expression of prestin, a membrane motor protein, in the mammalian auditory and vestibular periphery. Hear Res 184:27–40. [PubMed: 14553901]

Dechesne C 1992 The development of vestibular sensory organs in humanIn: Roman R, editor. Development of auditory and vestibular systems 2. Amsterdam: Elsevier p 419–447.

Desai SS, Zeh C, Lysakowski A. 2005 Comparative morphology of rodent vestibular periphery. I. Saccular and utricular maculae. J Neurophysiol 95:251–266.

Drescher DG, Ramakrishnan NA, Drescher MJ, Chun W, Wang X, Myers SF, Green GE, Sadrazodi K, Karadaghy AA, Poopat N, Karpenko AN, Khan KM, Hatfield JS. 2004 Cloning and characterization of alpha9 subunits of the nicotinic acetylcholine receptor expressed by saccular hair cells of the rainbow trout (*Oncorhynchus mykiss*). Neuroscience 127:737–752. [PubMed: 15283971]

Elgoyhen AB, Franchini LF. 2011 Prestin and the cholinergic receptor of hair cells: positively-selected proteins in mammals. Hear Res 273:100–108. [PubMed: 20056140]

Elgoyhen AB, Johnson DS, Boulter J, Vetter DE, Heinemann S. 1994 Alpha9: an acetylcholine receptor with novel pharmacological properties expressed in rat cochlear hair cells. Cell 79:705–715. [PubMed: 7954834]

Elgoyhen AB, Vetter DE, Katz E, Rothlin CV, Heinemann SF, Boulter J. 2001 Alpha10: a determinant of nicotinic cholinergic receptor function in mammalian vestibular and cochlear mechanosensory hair cells. Proc Natl Acad Sci U S A 98:3501–3506. [PubMed: 11248107]

Favre D, Sans A. 1979 Morphological changes in afferent vestibular hair cell synapses during the postnatal development of the cat. J Neurocytol 8:765–775. [PubMed: 541692]

Fernández C, Baird RA, Goldberg JM. 1988 The vestibular nerve of the chinchilla. I. Peripheral innervation patterns in the horizontal and superior semicircular canals. J Neurophysiol 60:167–181. [PubMed: 3404215]

Fernández C, Goldberg JM, Baird RA. 1990 The vestibular nerve of the chinchilla. III. Peripheral innervation patterns in the utricular macula. J Neurophysiol 63:767–780. [PubMed: 2341875]

Franchini LF, Elgoyhen AB. 2006 Adaptive evolution in mammalian proteins involved in cochlear outer hair cell electromotility. Mol Phylogenet Evol 41:622–635. [PubMed: 16854604]

Han GC, Lasker DM, Vetter DE, Minor LB. 2007 Extracellular recordings from semicircular canal afferents in mice that lack the alpha 9 acetylcholine receptor subunit [abstract]. ARO Midwinter Meeting, Denver p 1–2.

Happe HK, Morley BJ. 1998 Nicotinic acetylcholine receptors in rat cochlear nucleus: [^{125}I]-α-bungarotoxin receptor autoradiography and in situ hybridization of α7 nAChR subunit mRNA. J Comp Neurol 397:163–180. [PubMed: 9658282]

Hiel H, Elgoyhen AB, Drescher DG, Morley BJ. 1996 Expres-sion of nicotinic acetylcholine receptor mRNA in the adult rat peripheral vestibular system. Brain Res 738:347–352. [PubMed: 8955534]

Holt JC, Lioudyno M, Guth PS. 2003 A pharmacologically dis-tinct nicotinic ACh receptor is found in a subset of frog semicircular canal hair cells. J Neurophysiol 90:1526–1536. [PubMed: 12966175]

Holt JC, Lysakowski A, Goldberg JM. 2006 Mechanisms of efferent-mediated responses in the turtle posterior crista. J Neurosci 26:13180–13193. [PubMed: 17182768]

Holt JC, Lysakowski A, Goldberg JM. 2011 The efferent vestibular system In: Ryugo DK, Fay RR, Popper AN, editors. Springer handbook of auditory research: auditory and vestibular efferents, vol 38 New York: Springer Science & Business Media LLC p 135–186.

Holt JC, Kewin K, Jordan PM, Cameron P, Klapczynski M, McIntosh JM, Crooks PA, Dwoskin LP, Lysakowski A. 2015 Pharmacologically distinct nicotinic acetylcholine receptors drive efferent-mediated excitation in calyxbearing vestibular afferents. J Neurosci 35:3625–3643. [PubMed: 25716861]

Hübner PP, Khan SI and Migliaccio AA. 2015 The mammalian efferent vestibular system plays a crucial role in the high-frequency response and short-term adaptation of the vestibuloocular reflex. J Neurophysiol 114:3154–3165. [PubMed: 26424577]

Iwasaki S, Chicaro Y, Komuta Y, Ito K, Sahara Y. 2008 Low-voltage-activated potassium channels underlie the regulation of intrinsic firing properties of rat vestibular ganglion cells. J. Neurophysiol 100:2192–2204. [PubMed: 18632889]

Jones SM, Jones TA. 2014 Genetics of peripheral vestibular dysfunction: lessons from mutant mouse strains. J Am Acad Audiol 25:289–301. [PubMed: 25032973]

Jones SM, Erway LC, Bergstrom RA, Schimenti JC, Jones TA. 1999 Vestibular responses to linear acceleration are absent in otoconia-deficient C57Bl/6JEi-het mice. Hear Res 135:56–60. [PubMed: 10491954]

Jones SM, Erway LC, Johnson KR, Yu H, Jones TA. 2004 Gravity receptor function in mice with graded otoconial deficiencies. Hear Res 191:34–40. [PubMed: 15109702]

Jones TA, Jones SM, Colbert S. 1998 The adequate stimulus for avian short latency vestibular responses to linear translation. J Vestib Res 8:253–272. [PubMed: 9626651]

Jones TA, Jones SM, Vijayakumar S, Brugeaud A, Bothwell M, Chabbert C. 2011 The adequate stimulus for mammalian linear vestibular evoked potentials (VsEPs). Hear Res 280:133–140. [PubMed: 21664446]

Jones TA, Lee C, Gaines CG, Grant JW. 2015 On the high frequency transfer of mechanical stimuli from the surface of the head to the macular neuroepithelium of the mouse. J Assoc Res Otolaryngol 16:189–204. [PubMed: 25648882]

Jordan PM, Parks XX, Contini D, Holt JC. 2013 A review of synaptic mechanisms of vestibular efferent signaling in turtles: extrapolation to efferent actions in mammals. J Vestib Res 23:161–175. [PubMed: 24177348]

Jordan PM, Fettis M, Holt JC. 2015 Efferent innervation of turtle semicircular canal cristae: comparisons with bird and mouse. J Comp Neurol 523:1258–1280. [PubMed: 25560461]

Kalluri R, Xue J, Eatock RA. 2010 Ion channels set spike timing regularity of mammalian vestibular afferent neurons. J Neurophysiol 104:2034–2051. [PubMed: 20660422]

Karlin A 2002 Emerging structure of the nicotinic acetylcholine receptors. Nat Rev Neurosci 3:102–114. [PubMed: 11836518]

Kong WJ, Egg G, Hussl B, Spoendlin H, Schrott-Fischer A. 1994 Localization of ChAT-like immunoreactivity in the vestibular endorgans of the rat. Hear Res 75:191–200. [PubMed: 8071146]

Kong WJ, Guo CK, Zhang XW, Zhang S, Li GQ, Li ZW, Van Cauwenberge P. 2007 The coupling of acetylcholine-induced BK channel and calcium channel in guinea pig saccular type II vestibular hair cells. Brain Res 1129:110–115. [PubMed: 17157279]

Lathe R 2004 The individuality of mice. Genes Brain Behav 3:317–327. [PubMed: 15544575]

Le Novere N, Changeux J. 1995 Molecular evolution of the nicotinic acetylcholine receptor: an example of multigene family in excitable cells. J Mol Evol 40:155–172. [PubMed: 7699721]

Lipovsek M, Im GJ, Franchini LF, Pisciottano F, Katz E, Fuchs PA, Elgoyhen AB. 2012 Phylogenetic differences in calcium permeability of the auditory hair cell cholinergic nicotinic receptor. Proc Natl Acad Sci U S A 109:4311–4313.

Lipovsek M, Fierro A, Perez EG, Boffi JC, Millar NS, Fuchs PA, Katz E, Elgoyhen AB. 2014 Tracking the molecular evolution of calcium permeability in a nicotinic acetylcholine receptor. Mol Biol Evol 32:3250–3265.

Liu W, Davis RL. 2014 Calretinin and calbindin distribution patterns specify subpopulations of type I and type II spiral ganglion neurons in postnatal murine cochlea. J Comp Neurol. 522:2299–2318. [PubMed: 24414968]

Luebke AE, Maroni PD, Guth SM, Lysakowski A. 2005 Alpha-9 nicotinic acetylcholine receptor immunoreactivity in the rodent vestibular labyrinth. J Comp Neurol 492:323–333. [PubMed: 16217793]

Lustig LR, Peng H. 2002 Chromosome location and characterization of the human nicotinic acetylcholine receptor subunit alpha (alpha) 9 (CHRNA9) gene. Cytogenet Genome Res 98:154–159. [PubMed: 12697997]

Lustig LR, Hiel H, Fuchs PA. 1999 Vestibular hair cells of the chick express the nicotinic acetylcholine receptor subunit alpha 9. J Vestib Res 9:359–367. [PubMed: 10544374]

Lysakowski A 1996 Synaptic organization of the crista ampullaris in vertebrates. Ann N Y Acad Sci 781:164–182. [PubMed: 8694413]

Lysakowski A, Goldberg JM. 1997 A regional ultrastructural analysis of the cellular and synaptic architecture in the chinchilla cristae ampullares. J Comp Neurol 389:419–443. [PubMed: 9414004]

Lysakowski A, Goldberg JM. 2004 Morphophysiology of the vestibular periphery In: Highstein SM, Fay RR, Popper AN, editors. The vestibular system. New York: Springer p 57–152.

Lysakowski A, Goldberg JM. 2008 Ultrastructural analysis of the cristae ampullares in the squirrel monkey (*Saimiri sciureus*). J Comp Neurol 511:47–64. [PubMed: 18729176]

Mock B, Jones TA, Jones SM. 2011 Gravity receptor aging in the CBA/CaJ strain: a comparison to auditory aging. JARO 12:173–183. [PubMed: 21052761]

Morley B, Simmons D. 2012 Characterization of nicotinic acetylcholine receptor knockouts. ARO Abstr 35:263.

Morley BJ, Li HS, Hiel H, Drescher DG, Elgoyhen AB. 1998 Identification of the subunits of the nicotinic cholinergic receptors in the rat cochlea using RT-PCR and in situ hybridization. Brain Res Mol Brain Res 53:78–87. [PubMed: 9473597]

Morley BJ, Ohlemiller KK, Simmons DD. 2012 Efferent innervation and auditory function in constitutive and conditionally knocked out α9 nAChR mice. Program No. 137.03. New Orleans Society for Neuroscience, Online.

Nazareth AM, Jones TA. 1998 Central and peripheral components of short latency vestibular responses in the chicken. J Vestib Res 8:233–252. [PubMed: 9626650]

Plazas PV, Katz E, Gomez-Casati ME, Bouzat C, Elgoyhen AB. 2005 Stoichiometry of the α9α10 nicotinic cholinergic receptor. J Neurosci 25:10905–10912. [PubMed: 16306403]

Pujol R, Pickett SB, Nguyen TB, Stone JS. 2014 Large basolateral processes on type II hair cells are novel processing units in mammalian vestibular organs. J Comp Neurol 522:3141–3159. [PubMed: 24825750]

Rabbitt RD, Brownell WE. 2011 Efferent modulation of hair cell function. Curr Opin Otolaryngol Head Neck Surg 19:376–381. [PubMed: 22552698]

Ramakrishnan NA, Drescher MJ, Morley BJ, Kelley PM, Drescher DG. 2014 Calcium regulates molecular interactions of otoferlin with SNARE proteins required for hair cell exocytosis. J Biol Chem 289:8760–8766.

Rothman JS, Manis PB. 2003 The roles potassium currents play in regulating the electrical activity of ventral cochlear nucleus neurons. J Neurophysiol 89:3097–3113. [PubMed: 12783953]

Sadeghi SG, Minor LB, Cullen KE. 2007 Response of vestibular-nerve afferents to active and passive rotations under normal conditions and after unilateral labyrinthectomy. J Neurophysiol 97:1503–1514. [PubMed: 17122313]

Schug N, Braig C, Zimmermann U, Engel J, Winter H, Ruth P, Blin N, Pfister M, Kalbacher H, Knipper M. 2006 Differential expression of otoferlin in brain, vestibular system, immature and mature cochlea of the rat. Eur J Neurosci 24:3372–3380. [PubMed: 17229086]

Schweizer FE, Savin D, Luu C, Sutemeier DR, Hoffman LF. 2009 Distribution of high-conductance calcium-activated potassium channels in rat vestibular epithelia. J Comp Neurol 517:134–45. [PubMed: 19731297]

Selyanko AA, Hadley JK, Wood IC, Abogadie FC, Jentsch TJ. 2000 Inhibition of KCNQ1-4 potassium channels expressed in mammalian cells via M1 muscarinic acetylcholine receptors. J Physiol 522:349–355. [PubMed: 10713961]

Simmons DD, Morley BJ. 1998 Differential expression of the alpha9 nicotinic acetylcholine receptor subunit in neonatal and adult cochlear hair cells. Brain Res Mol Brain Res 56:287–292. [PubMed: 9602155]

Simmons DD, Morley BJ. 2011 Spatial and temporal expression patterns of nicotinic acetylcholine α9 and α10 subunits in the embryonic and early postnatal inner ear. Neuroscience 194:326–336. [PubMed: 21843604]

Smith M, Souza FO, Bruce K, Strang C, Morley BJ, Keyser K. 2014 Acetylcholine receptors in the retinas of the alpha7 nicotinic acetylcholine receptor knockout mouse. Mol Vis 20:1328–1356. [PubMed: 25352741]

Vetter DE, Liberman MC, Mann J, Barhanin J, Boulter J, Brown MC, Saffiote-Kolman J, Heinemann SF, Elgoyhen AB. 1999 Role of alpha9 nicotinic ACh receptor subunits in the development and function of cochlear efferent innervation. Neuron 23:93–103. [PubMed: 10402196]

Vetter DE, Katz E, Maison SF, Taranda J, Turcan S, Ballestero J, Liberman MC, Elgoyhen AB, Boulter J. 2007 The α10 nicotinic acetylcholine receptor subunit is required for normal synaptic function and integrity of the olivocochlear system. Proc Natl Acad Sci U S A 104:20594–20599. [PubMed: 18077337]

Wersäll J 1956 Studies on the structure and innervation of the sensory epithelium of the cristae ampullaris in the guinea pig: A light and electron microscopic investigation. Acta Otolaryngol Suppl 126:1–85. [PubMed: 13326368]

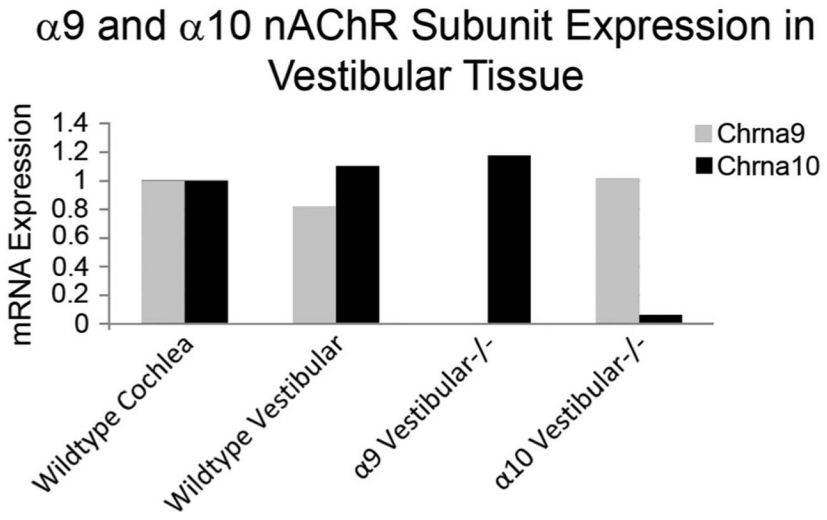

Figure 1.

Customized PCR arrays (Qiagen) were used to quantify α9 and α10 nicotinic receptor subunit expression at birth in cochlear and vestibular tissue samples to confirm loss of transcript in the knockouts. Cochlear transcripts were used as the positive control and assigned a value of 1. Transcript in vestibular tissue was compared to that in the cochlea. Primers designed for PCR arrays may amplify unrelated transcripts when the gene for which the primers were designed is absent. We sequenced the product from wild-type tissue to verify that the amplified products were α9 and α10. All products for α9 and α10 in the knockout tissues were also sequenced, and some small quantities of multiple unrelated transcripts were found. Primers may amplify nonrelated transcripts in the absence of gene expression (gene deletion). The quantity of irrelevant PCR product obtained with the α9 primers in the α9 knockout is barely detectable and is not visible in this graph, although the corresponding irrelevant PCR product in the α10 knockout is visible.

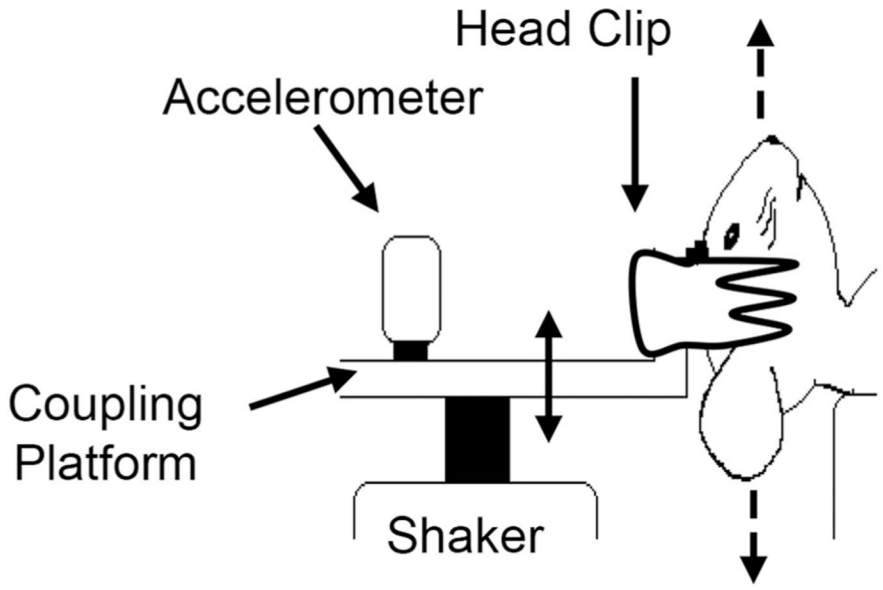

Figure 2.

Linear translation stimuli are presented in the naso-occipital cranial axis (dashed arrows) to elicit vestibular sensory evoked potentials. Anesthetized animals were placed supine, and the head was coupled to the electromechanical shaker and platform using a spring-loaded clip. A calibrated accelerometer was mounted to the platform to monitor stimuli.

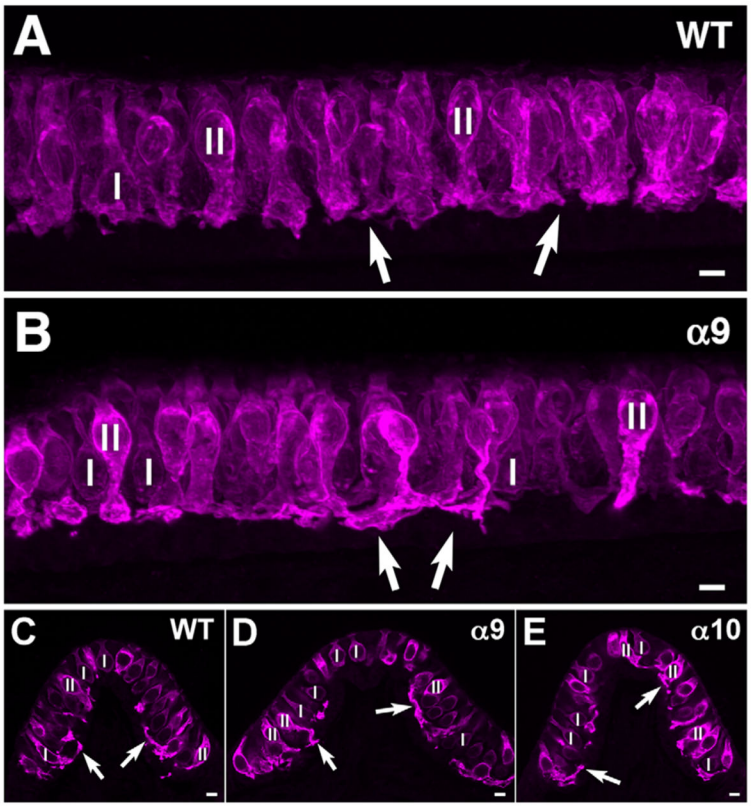

Figure 3.

Otoferlin (magenta) marks hair cells in the utricular macula and crista; it labels type II hair cells more intensely than type I hair cells. The two types can be distinguished by the levels of their nuclei: type I HC nuclei (I) are usually located more basally, whereas type II HC nuclei (II) are located more apically. Type II hair cells frequently have extended foot processes (arrows), as is the case here also (see text). **A**: Wild-type utricle. **B**: α9 KO utricle. **C**: Wild-type crista. **D**: α9 KO crista. **E**: α10 KO crista. Note the similar appearance of the hair cells in all photographs. Scale bars = 5 μm.

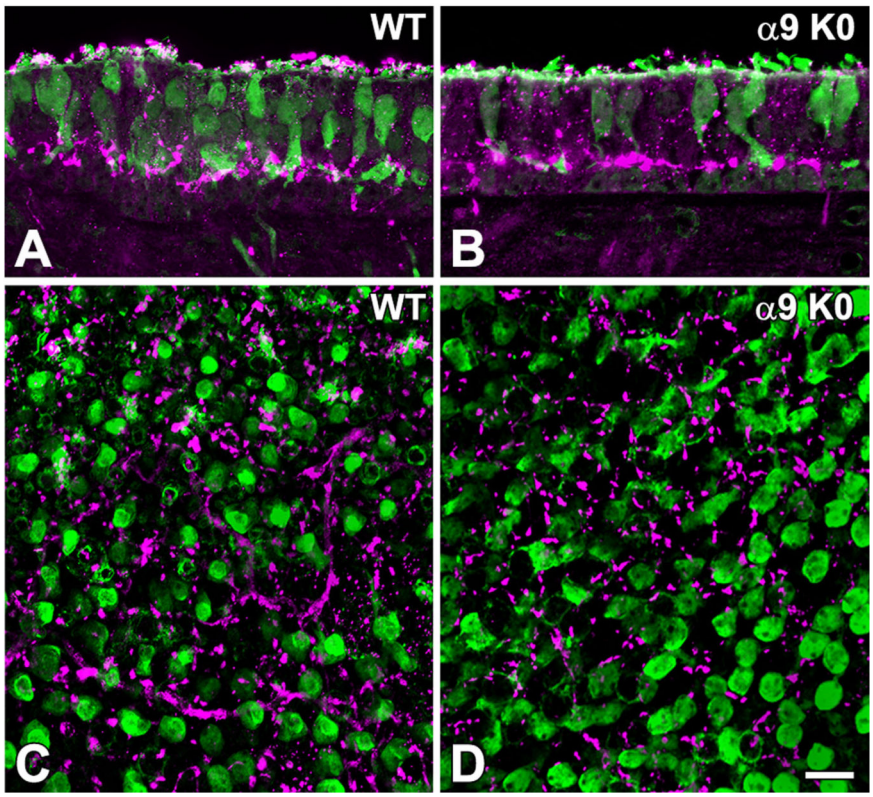

Figure 4.

Choline acetyltransferase (ChAT) was used to mark efferent boutons (magenta) synapsing on calretinin-labeled type II hair cells (green) and calyces surrounding type I hair cells in short stacks of sections (**A,B**) and in whole mounts (**C,D**) of utricular maculae in WT (A,C) and a9 KO (B,D) mice. Open profiles in C and D are the calyx endings of pure calyx afferents (green) in the striolar region. A and B are maximum intensity projections of six-section stacks of optical sections. C and D are 3D renderings of image stacks, obtained with Zeiss Zen software, using the “transparency” option. As can be observed, the number, location, and appearance of efferent boutons are similar in both strains of mice. Scale bar = 10 μm.

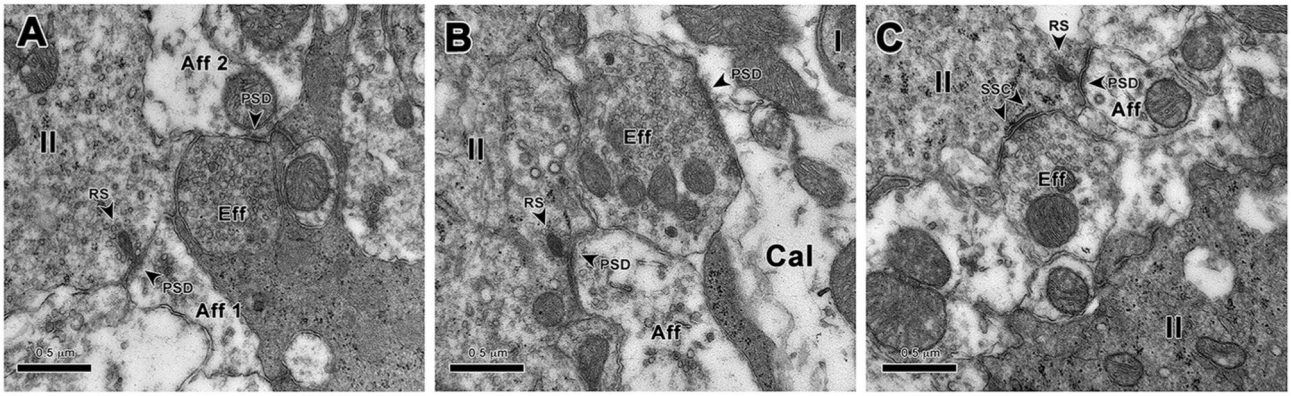

Figure 5.

Ultrastructure of efferent boutons in macular sensory epithelium. **A**: Ultrathin section of utricular macula from a wild-type (WT) mouse illustrating both afferent and efferent synaptic innervation. Afferent bouton 1 (Aff1) contains a postsynaptic density (PSD) opposite a ribbon synapse (RS) that it receives from a type II hair cell (II). Afferent bouton 2 (Aff2) is receiving a synapse indicated by the PSD, from the efferent bouton (Eff). **B**: Ultrathin section from the utricular macula of an α9 mouse. Similar to the case for WT mouse shown in A, a type II hair cell provides a normal-looking ribbon synapse (RS) to an afferent bouton (Aff), which contains a PSD. Efferent innervation also appears similar to the WT, with an efferent bouton (Eff) synapsing by means of a PSD on a calyx ending (Cal) surrounding a type I hair cell (I). **C**: In the α9 KO, an efferent bouton (Eff) making direct contact with a type II hair cell does so by means of a typical subsynaptic cistern-type synapse (SSC). Scale bars = 0.5 µm.

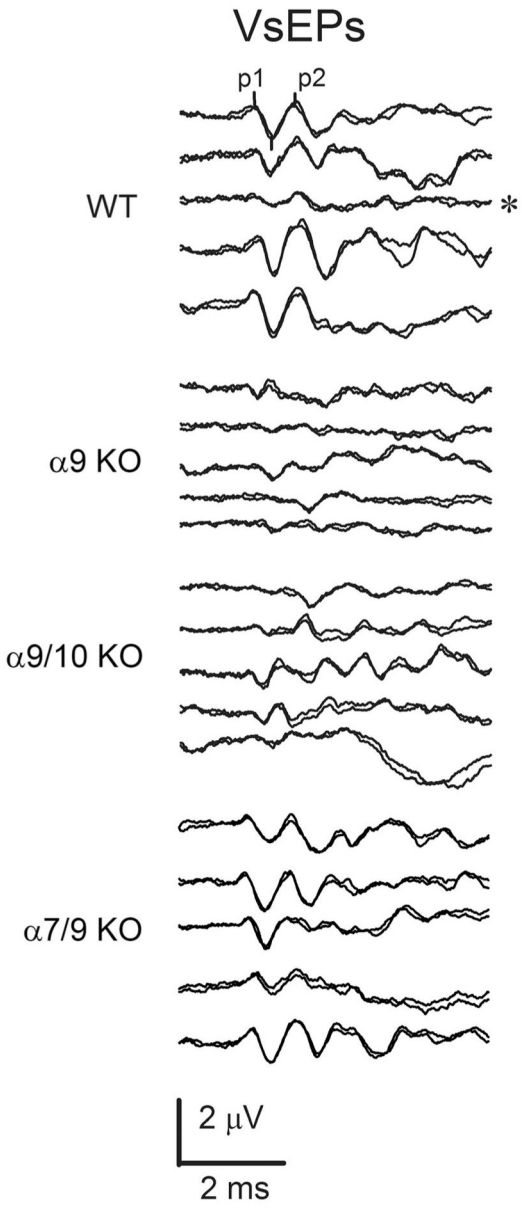

Figure 6.

VsEP waveforms. VsEP measurements were made in wild-type (WT), α9 KO, α9/10 KO, and α7/9 KO mice. VsEP waveforms shown were produced in response to the maximum level stimulation (+6 dB re:1 g/msec). The first three peaks are marked in the first pair of responses representing p1, n1, and p2 (n1 is marked but not labeled here). The WT animals produced responses with normal morphology and moderate variation in amplitudes and latencies. WT waveforms generally had well-formed, highly reproducible P1 and P2 response peaks. The WT response pair marked with an asterisk has unusually low amplitudes and was the only example of such poor amplitude in WT animals. The remaining four examples of WT waveforms demonstrate the typical variation seen among normal animals. VsEP waveforms of the α7/9 KO group (bottom five trace pairs labeled α7/9 KO) also had well-formed responses comparable to those of WT animals. In contrast, response

waveforms for both α9 and α9/10 animals were far more variable, where amplitudes ranged from those comparable to normal WT animals to very low amplitudes, including absent or virtually absent responses in α9 KOs (e.g., traces pairs 2 and 5 of α9 KO group). Examples of such poorly formed responses from α9 KO and α9/10 KO animals are shown as the middle 10 response trace-pairs (labels α9 KO and α9/10 KO). Responses of many α9 KO and α9/10 KO animals exhibited peaks with unusually short latency and duration. Examples of this can be seen, especially in α9/10 KO animals.

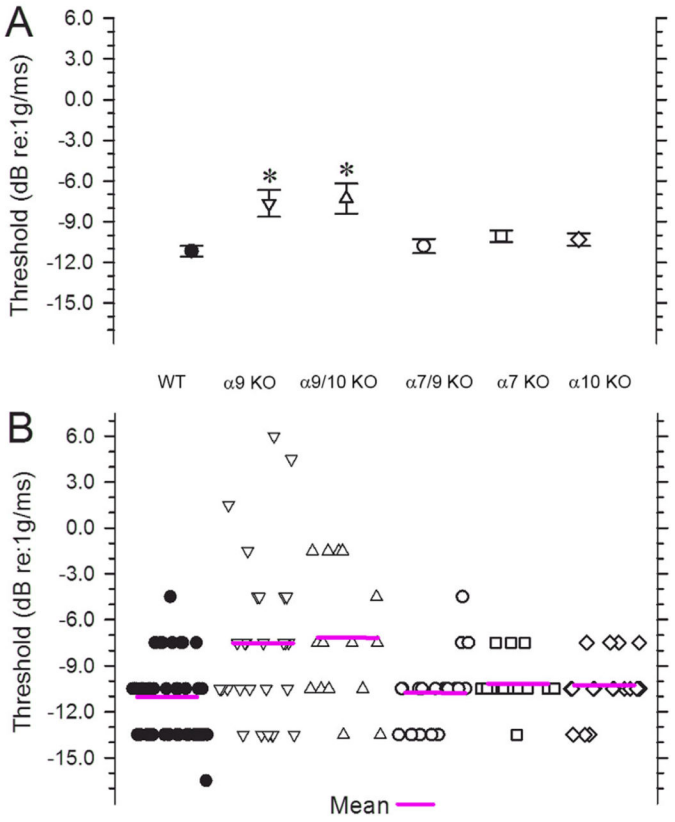

Figure 7.

VsEP thresholds. **A**: Mean (magenta lines) and SE for VsEP thresholds. **B**: The distribution of thresholds in individual animals for the six genotypes is shown (WT, α9 KO, α9/10 KO, α7/9 KO, α7 KO, and α10 KO). Mean thresholds for α9 KO and α9/10 KO animals were significantly higher (*$P < 0.0002$) than in WT animals. In contrast, there was no significant difference in thresholds between WT and α7/9 KO animals, nor was there a difference between threshold means for α9 KO and α9/10 KO animals.

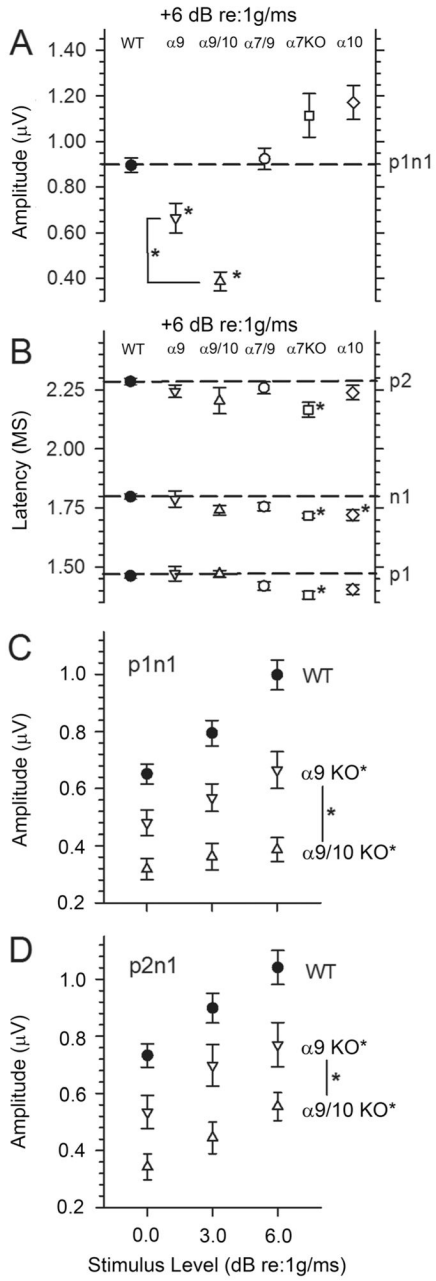

Figure 8.

VsEP amplitudes. **A**: Normalized p1n1 amplitudes for responses recorded at the highest stimulus level (+6 dB re:1 g/msec). WT (solid circles), α9 KO (downward triangles) and α9/10 KO (upward triangles), α7/9 KO (open circles), α7 KO (squares), and α10 KO (diamonds) are shown. Amplitudes for p1n1 were significantly reduced for both α9 KO and α/10 KO groups at +6 dB re:1 g/msec (significance indicated with an asterisk; $*P < 0.007$). Amplitudes of α9/10 KO animals were also lower than those of α9 KO animals (asterisk). At the highest stimulus level, the amplitude of p2n1 was also significantly reduced compared with WT for α9/10 KO animals (not shown in A; see D). **B**: VsEP latencies for p1, n1, and p2 at the highest stimulus levels (+6 dB re:1 g/msec). WT, α9/10 KO, α9/10 KO, α7/9

KO, α7 KO, and α10 KO are represented. Peripheral latencies (p1, n1) were either the same or significantly shorter than in WT knockout groups. The shortest latencies were found in α7 KO and α10 KO animals (*$P < 0.003$). **C,D**: p1n1 (C) and p2n1 (D) amplitudes at the three highest stimulus levels (0, +3, +6 dB re:1 g/msec). Both α9 KO and α9/10 KO mice consistently had significantly reduced amplitudes (*$P < 0.0031$) compared with WT, and α9/10 KO amplitudes were less than α9 KO amplitudes (*$P < 0.021$).

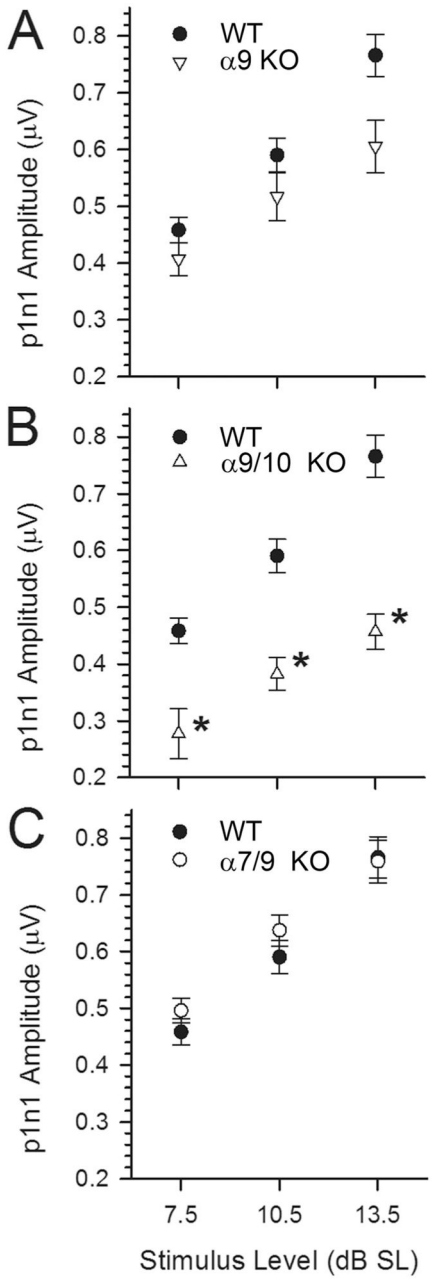

Figure 9.

VsEP amplitudes for p1n1 at three stimulus levels, +7.5, +10.5, and +13.5 dB above threshold (expressed in dB SL). Note that amplitudes increase systematically with increasing stimulus level in all genotypes. For the α9 KO animals (**A**; α9 KO), amplitudes are comparable to those of WT animals when stimulus level is expressed relative to each animal's threshold (dB SL). This is true despite significantly reduced p1n1 amplitudes at the highest absolute stimulus level as shown in Figs. 7A,C,D, suggesting that the reduced amplitudes in the α9 KO group are due largely to threshold changes. In contrast, amplitude differences between WT and α9/10 KOs (**B**) were somewhat reduced in Figure 7A but remained significantly lower than WT when plotted against dB SL here (*P< 0.0003). Thus,

differences in threshold were not entirely responsible for decreases in VsEP amplitudes for the α9/10 KO group. There were no significant differences in p1n1 and p2n1 (not shown) amplitudes between WT and α7/9 KO groups (**C**).

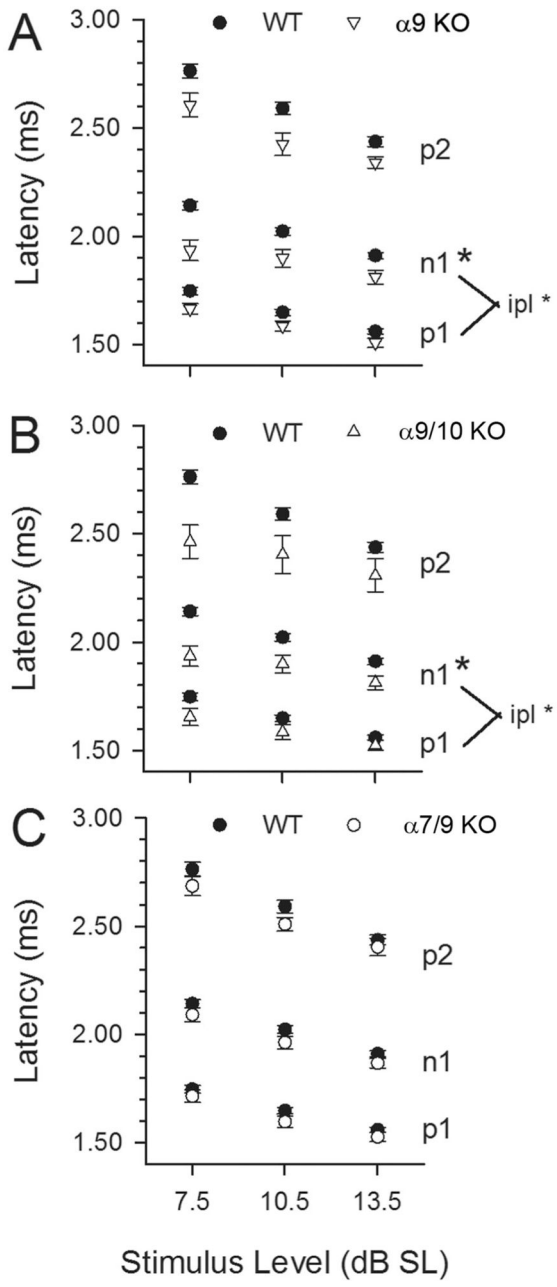

Figure 10.

VsEP Latencies for p1, n1, and p2 at three stimulus levels expressed relative to threshold (+7.5, +10.5, +13.5 dB SL). WT (solid circles), α9 KO (downward triangles), α9/10 KOs (upward triangles), and α7/9 KO (open circles) groups are represented in **A-C**, respectively. At the highest stimulus levels (cf. Fig. 7B; +6 dB re:1 g/msec), peripheral latencies (p1, n1) of α9 KO, α9/10 KO and α7/9 KO were the same as WT. When expressed relative to threshold (as shown here) over several stimulus levels (+7.5, +10.5 and +13.5 dB above threshold, i.e., dB SL), latency differences were more pronounced in α9 KO and α9/10 KO animals, both of which had significantly reduced n1 latencies and shorter interpeak latencies for peripheral peaks (p1 minus n1, $*P < 0.005$). Also noted are significantly shorter latencies

for α7 KO and α10 KO compared with WT animals. Latencies for α7/9 KO mice remained approximately the same when expressed in relation to threshold (dB SL).

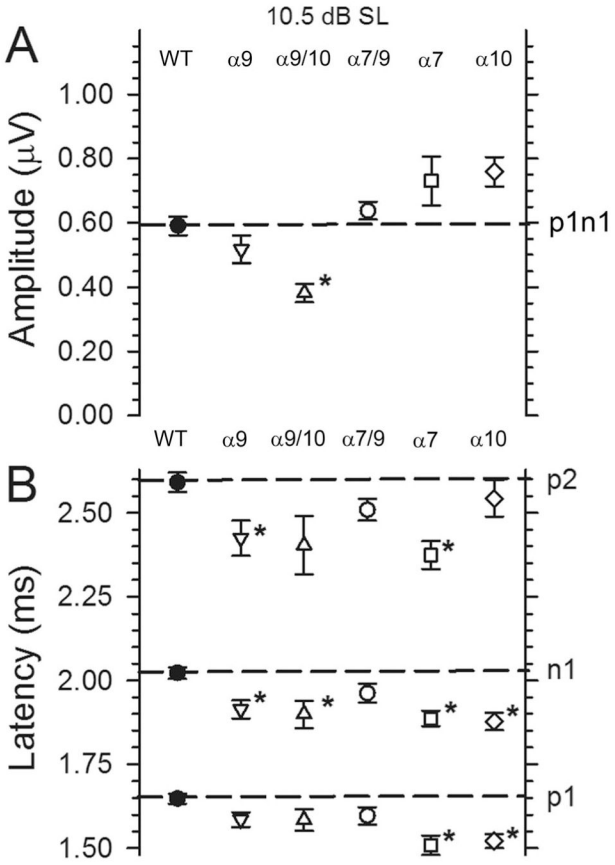

Figure 11.

A,B: VsEP amplitudes and latencies recorded at +10.5 dB above threshold (dB SL) for all genotypes. This facilitates comparison of response features across all genotypes. Note that amplitudes were significantly reduced (**P* < 0.003) compared with WT only in α9/10 KO animals, whereas significantly shorter n1 latencies were resolved for α9 KO, α9/10 KO, α7 KO, and α10 KO animals. n1 Latencies remain the same as WT only in α7/9 KO animals.

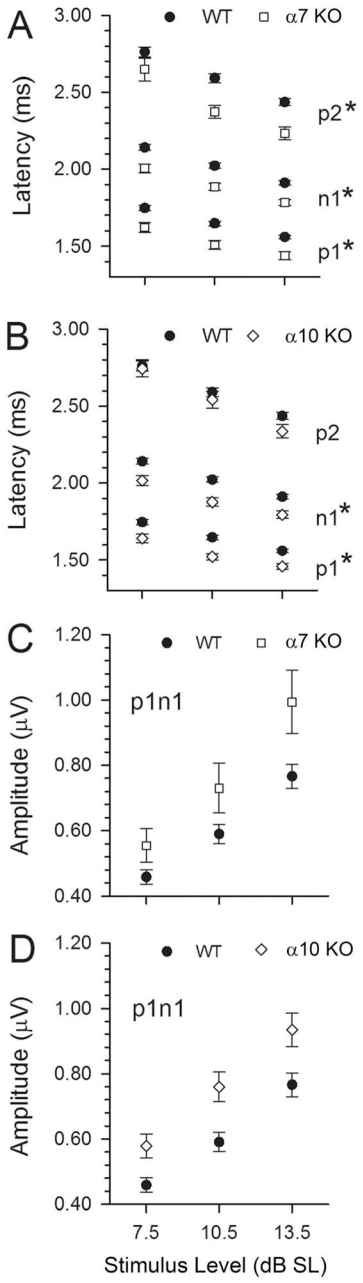

Figure 12.

Detailed VsEP latency (**A,B**) and amplitude (**C,D**) characteristics for α7 KO and α10 KO mice obtained at three stimulus levels (+7.5, +10.5, and +13.5 dB SL). Significantly shorter latencies (A,B) were consistently observed in α7 KO and α10 KO animals (*$P < 0.002$). Interestingly, interpeak latencies were no different from WT in these genotypes. Robust amplitudes (C,D) were also characteristic of the α7 KO and α10 KO mice, although they were not significantly larger than WT.

GENOME SCAN FOR WILD TYPE AND KNOCKOUT MICE WITH THE "BEST" AND "WORST" THRESHOLDS FOR CHROMOSOME 5 (α9) AND CHROMOSOME 7 (α10)

Marker	Chr	Start bp	2013	2038	1099	2012	2048	2055	303	343	326	346	348	C57BL/6J	129SvJ
Chr5-1	5	7461340	1	1	1	1	1	1	1	1	1	1	1	1	0
Chr5-2	5	12837850	1	1	1	1	1	1	1	1	1	1	1	1	1
Chr5-3	5	20532162	1	1	1	1	1	1	1	1	1	1	1	1	0
Chr5-4	5	28888081	1	1	1	1	1	1	1	1	1	1	1	1	1
Chr5-5	5	33329619	1	1	1	1	1	1	1	1	1	1	1	1	0
Chr5-6	5	42600456	1	1	1	1	1	1	1	1	1	1	1	1	1
Chr5-7	5	50966233	0	0	0	0	0	0	0	0	0	0	0	1	0
Chr5-8	5	58107090	1	1	1	1	1	1	1	1	1	1	1	1	1
Chr5-9	5	68029080	0	0	0	0	0	0	0	0	0	0	0	1	0
Chr5-10	5	73033762	1	1	1	1	1	1	1	1	1	1	1	1	1
Chr5-11	5	78253018	0.5	0	0	0	0	0	0	0	0	0	0	1	0
Chr5-12	5	86787409	1	1	1	1	1	1	1	1	1	1	1	1	1
Chr5-13	5	91904489	0.5	0	0.5	0	0.5	0.5	0	0	0	0	0	1	0
Chr5-14	5	100829662	1	1	1	1	1	1	1	1	1	1	1	1	1
Chr5-15	5	104572764	0	0	0.5	0	0.5	0.5	0	0	0	0	0	1	0
Chr5-16	5	114660997	1	1	1	1	1	1	1	1	1	1	1	1	1
Chr5-17	5	119758227	0	1	1	1	1	1	0	0	0	0	0	1	0
Chr5-18	5	123738720	1	1	1	1	1	1	1	1	1	1	1	1	1
Chr5-19	5	131210820	1	1	1	1	1	1	1	1	1	1	1	1	0
Chr5-20	5	137222873	1	1	1	1	1	1	1	1	1	1	1	1	1
Chr5-21	5	145631811	1	1	1	1	1	1	1	1	1	1	1	1	0
Chr5-22	5	151148537	1	1	1	1	1	1	1	1	1	1	1	1	1

Chr7-15	7	109389815	1	1	1	1	1	1	0	0	0	0	0	1	0
Chr7-16	7	121418263	1	1	1	1	1	1	1	1	1	1	1	1	1
Chr7-17	7	125673109	1	1	1	1	1	1	0	0	0	0	0	1	0
Chr7-18	7	134597736	1	1	1	1	1	1	1	1	1	1	1	1	1
Chr7-19	7	140062817	1	1	1	1	1	1	0	0	0	0	0	1	0
Chr7-20	7	145329120	1	1	1	1	1	1	1	1	1	1	1	1	1
Chr7-21	7	152082670	1	1	1	1	1	1	1	1	1	1	1	1	0
Chr7-22	7	152494066	1	1	1	1	1	1	1	1	1	1	1	1	1

Figure 13.

The amount of 129/sv background flanking CHRNA9 (upper panel) and CHRNA10 (lower panel) was determined by using SNPs, as described in Materials and Methods, for several α9 KO and double α9/10 KOs with the "best" and "worst" thresholds. Along the y-axis is shown the marker, chromosome (Chr), and starting base pair (bp). CHRNA9 is located on chromosome 5 (upper panel), and CHRNA10 is located on chromosome 7 (lower panel) in the mouse. Along the top are the animal numbers. Animal numbers in green had the best thresholds and animals in pink had the worst thresholds. Zero (yellow) is 129/sv, and 1 (blank) is C57Bl/6J background. The 0.5 indicates heterozygotes. The animals with the best threshold (2038) and the worst threshold (2012) have an identical strain characterization pattern. This analysis cannot eliminate all genetic effects on the phenotype; for example, it cannot eliminate genes closely linked to *CHRNA9* or *CHRNA10*.

TABLE 1.

Antibody Labeling

Antibody (dilution)	Immunogen	Source, host, catalog No., clone or lot No., RRID	Validation	Staining pattern
Anticholine acetyltransferase (1:200)	Human placental enzyme	Chemicon/EMD-Millipore, goat polyclonal, AB144P, NG1915294, AB_2079751	Western blot (immunoblot; Jordan et al., 2015)	Mammalian vestibular efferents (Kong et al., 1994; Jordan et al. 2015)
Anticalretinin (1:200)	Recombinant rat calretinin	Chemicon/EMD-Millipore, rabbit polyclonal, B1550, 60302, AB_90764	Western blot (immunoblot; Liu and Davis, 2014)	Mammalian type II vestibular hair cells and afferents (Desai et al., 2005; Jordan et al., 2015)
Antiotoferlin (1:800)	Recombinant mouse peptide 1238-1391 (GenBank accession No. AAG12990)	Thermo Fisher Scientific, rabbit polyclonal, Custom_MorBar_001, AB_2616561	Western blot (immunoblot; Ramakrishnan et al., 2014)	Mammalian cochlear and vestibular hair cells (Ramakrishnan et al., 2014); consistent with in situ hybridization pattern (Schug et al., 2006)

TABLE 2.

VsEP Thresholds and Amplitudes[1]

Genotype	Threshold (dB re:1 g/msec)	p1n1 (μV)	p2n1 (μV)
WT	−11.18 ± 2.58 (44)	0.998 ± 0.344 (44)	1.041 ± 0.391 (43)
α9 KO	−7.66 ± 5.30 (28)[3]	0.665 ± 0.333 (26)[3]	0.771 ± 0.389 (25)[2]
α9/10 KO	−7.30 ± 4.31 (15)[3]	0.387 ± 0.161 (15)[3]	0.554 ± 0.186 (14)[3]
α7/9 KO	−10.80 ± 2.36 (20)	0.924 ± 0.213 (20)	0.829 ± 0.234 (20)
α7 KO	−10.07 ± 1.60 (14)	1.114 ± 0.360 (14)	1.196 ± 0.395 (14)
α10 KO	−10.33 ± 1.92 (18)	1.172 ± 0.316 (18)	1.187 ± 0.311 (18)

[1]Values are mean ± SD (n); thresholds and amplitudes (p1n1 and p2n1) were obtained at the highest stimulus level (+6 dB re:1 g/msec). Statistical tests for thresholds (ANOVA, $F_{5,33} = 5.865$, $P = 6.3 \times 10^{-5}$; LSD: α9 KO: $P = 2.9 \times 10^{-5}$, α9/10 KO: $P = 1.8 \times 10^{-4}$), Response amplitudes at the highest stimulus level (MANOVA, $F_{10,256} = 7.709$, $P = 8.9 \times 10^{-11}$, LSD: p1n1: α9 KO, $P = 4.9 \times 10^{-5}$, α9/10 KO, $P = 2.43 \times 10^{-9}$; p2n1: α9 KO, $P = 0.0022$, α9/10 KO, $P = 1.0 \times 10^{-5}$), and response amplitudes at the three highest levels (0, +3, and +6 dB re:1 g/msec: rmMANOVA, $F_{10,250} = 6.53$, $P = 5.7 \times 10^{-9}$; LSD: α9 KO, p1n1: $P = 2.08 \times 10^{-4}$; p2n1: $P = 0.003$; LSD: α9/10 KO, p1n1: $P = 1.22 \times 10^{-8}$; p2n1: $P = 1.0 \times 10^{-6}$) were significantly reduced in the α9 KO and α9/10 KO. Amplitudes for the α9/10 KOs tended to be less than those of α9 KOs (+6 dB re:1 g/msec, MANOVA, $F_{10,256} = 7.709$, $P = 8.9 \times 10^{-11}$, LSD: p1n1: $P = 0.0067$).

[2]$P < 0.003$.

[3]$P < 0.001$.

TABLE 3.

VsEP Latencies[1]

Genotype	p1 (μsec)	n1 (μsec)	p2 (μsec)
WT	1,463 ± 72 (44)	1,798 ± 79 (44)	2,286 ± 91 (43)
α9 KO	1,472 ± 154 (26)	1,788 ± 174 (26)	2,244 ± 132 (25)
α9/10 KO	1,471 ± 57 (15)	1,741 ± 79 (15)	2,204 ± 206 (14)
α7/9 KO	1,420 ± 78 (20)	1,755 ± 76 (20)	2,259 ± 113 (20)
α7 KO	1,381 ± 63 (14)[2]	1,718 ± 40 (14)[2]	2,166 ± 119 (14)[2]
α10 KO	1,405 ± 89 (18)	1,720 ± 96 (18)[2]	2,238 ± 130 (18)

[1]Values are mean ± SD (n); latencies were obtained at the highest stimulus level (+6 dB re:1 g/msec). Statistical tests for neural activation latencies at the highest stimulus level (+6 dB; MANOVA, $F_{15,384} = 3.344$, $P = 2.6 \times 10^{-5}$; LSD: p1: α7 KO, $P = 9.4 \times 10^{-4}$; n1: α7 KO, $P = 0.0024$; α10 KO, $P = 0.0013$; p2: α7 KO, $P = 0.0024$) and for latencies across the three highest stimulus levels (0, +3, and +6 dB re:1 g/msec; rmMANOVA, $F_{15,375} = 5.41$, $P = 6.4 \times 10^{-10}$; p1: α7 KO, $P = 5.2 \times 10^{-4}$, α10 KO, $P = 1.1 \times 10^{-3}$). Peripheral latencies for α7 KO and α10 KO (rmMANOVA, $F_{15,333} = 5.04$, $P = 5.48 \times 10^{-9}$; LSD: α7 KO, p1: $P = 2.4 \times 10^{-5}$, n1: $P = 8.3 \times 10^{-5}$, p2: $P = 1.3 \times 10^{-3}$; α10 KO: p1: $P = 4.6 \times 10^{-5}$, n1: $P = 1.4 \times 10^{-5}$) were significantly lower than in the other groups.

[2]$P < 0.003$.